

Remote sensing of aerosols with the Earth Observing Scanning Polarimeter

Larry D. Travis

NASA Goddard Space Flight Center  
Goddard Institute for Space Studies  
2880 Broadway, New York, NY 10025

**ABSTRACT**

Tropospheric aerosols have potential climate forcing roles through both the direct effect on solar radiation scattered and absorbed and the indirect effect as condensation nuclei for cloud particles. Present capabilities for characterizing the global aerosol climatology are limited by the existing satellite remote sensing measurements, making a quantitative determination of the climate forcing effects of aerosols rather difficult and uncertain. The Earth Observing Scanning Polarimeter (EOSP) instrument under consideration for Earth Observing System (EOS) mission platforms and for a proposed Climsat Earth Probe mission is intended to provide global mapping with multispectral photopolarimetry, which can be exploited for the more pronounced aerosol signature in the polarization of the scattered light as compared to the radiance. We describe the essential features and performance specifications of the EOSP instrument and discuss approaches for retrieving tropospheric aerosol properties from multispectral photopolarimetry.

**1. INTRODUCTION**

From the perspective of most past and present terrestrial remote sensing efforts, atmospheric aerosols represent a nuisance that necessitates developing and applying procedures for removing their contribution to the radiance measured by the satellite sensor in order to obtain the desired radiance characteristics of land-vegetation or ocean. There is, however, increasing interest in the aerosols themselves because of the role that they may play in contributing to global climate change, particularly in view of the increase in the anthropogenic sulfate component due to industrial emissions of  $\text{SO}_2$ . Tropospheric aerosols have a direct radiative forcing effect due simply to their scattering and absorption of solar radiation and also an indirect effect as cloud condensation nuclei and the resulting potential for modifying the shortwave reflectivity of the clouds. Charlson et al.<sup>1</sup> point out that sulfate aerosols tend to increase planetary albedo through both direct and indirect effects; they estimate the average cooling due to the anthropogenic sulfate component to be of order 1 to 2  $\text{W m}^{-2}$  and note that this is a cooling rate similar in magnitude to the present anthropogenic greenhouse gas warming. Of course, there is great diversity in type, source, and distribution of aerosols, and in some cases the specific aerosol component can produce warming rather than cooling. An adequate understanding of the climate forcing role and any systematic trends will depend upon an integrated program that includes satellite remote sensing to provide routinely a global climatology of aerosols.

Efforts to develop techniques for removing aerosol effects from Coastal Zone Color Scanner radiances have led to some attempts to retrieve aerosol information,<sup>2</sup> but the only operational product at present is the aerosol optical thickness obtained using channel-1 (0.58-0.68  $\mu\text{m}$ ) radiances from the Advanced Very High Resolution Radiometer (AVHRR) on the NOAA polar orbiting environmental satellites.<sup>3</sup> With single channel

AVHRR data, one must use an approach which is based on the increase in observed radiance owing to greater scattering from optically thicker aerosol layers and is suited only for situations where the surface has a low albedo that is well known *a priori*. Thus, the NOAA operational product is restricted to coverage over the ocean at AVHRR scan angles well away from sun glint, and may nonetheless be subject to ambiguity caused by optically thin or subpixel clouds. Efforts to develop techniques which use multispectral radiances<sup>3,4</sup> or surface feature contrast sensitivity<sup>5,6</sup> have been pursued by various investigators with the goal of improving aerosol detection sensitivity and coverage as well as extending remote sensing retrievals to aerosol properties in addition to optical thickness.

Interestingly, remote sensing of aerosols for planets other than the Earth is somewhat more advanced due largely to approaches based upon utilizing the significant additional information content on aerosol and cloud properties when the radiance measurements are supplemented with the polarization. The effectiveness of using polarimetry as a remote sensing tool was first convincingly demonstrated by the analyses of ground-based observations of Venus.<sup>7,8</sup> Since then spacecraft observations from polarimeters on the Pioneer 10 and 11 missions have provided information on aerosols on Jupiter,<sup>9</sup> Saturn,<sup>10</sup> and Titan,<sup>11</sup> and on Venus from the Pioneer Venus Orbiter mission.<sup>12</sup> Prompted by the demonstrated effectiveness of polarimetry from planetary missions, we have developed an instrument design for the EOSP intended to make multispectral radiance and linear polarization degree measurements in order to produce key components of a global climatology of tropospheric aerosols. This instrument is under consideration for flight on the second of the series of AM platforms of EOS and for a proposed Climsat Earth Probe mission.

## 2. INSTRUMENT DESIGN

In order to realize the full potential for aerosol retrieval using multispectral photopolarimetry, we required an EOSP design which incorporated the following key features: (1) simultaneous detection of orthogonal polarization components of the scene radiance; (2) capability to interchange the roles of corresponding detector elements used to detect orthogonal polarization components; (3) spatial coverage from limb to limb to provide global polarization maps; (4) simultaneous measurement in all twelve spectral bands; (5) instrumental polarization that is small and varies only slightly with scan angle along with a method to measure the instrumental polarization in flight as well as pre-flight; (6) single instantaneous field of view (IFOV) for all spectral bands and polarization components; and (7) inflight calibration sources and methods adequate to provide radiometric calibration and polarimetric calibration.

Figure 1 displays a cut-away view of the basic instrument design. A scanning system provides a continuous sweep of the IFOV in the direction perpendicular to the spacecraft ground track, allowing limb-to-limb coverage and calibration source viewing plus dc-restoration during the backscan portion of the 360° rotation. The scan mirror assembly, shown in more detail in Fig. 2, employs a pair of protected silver coated mirrors mounted in a carrying tube. By utilizing a pair of 45° incidence angle mirrors with their respective incidence-reflection planes orthogonal to each other, we have a cancellation of the instrumental polarization components imposed upon the scene flux by the non-normal reflection at each mirror. Thus, the overall instrumental polarization is small if the mirrors are identical. Fabrication of the mirrors so that they are very nearly identical is straightforward, with the most obvious approach simply being the coating of both mirrors in the same deposition run.

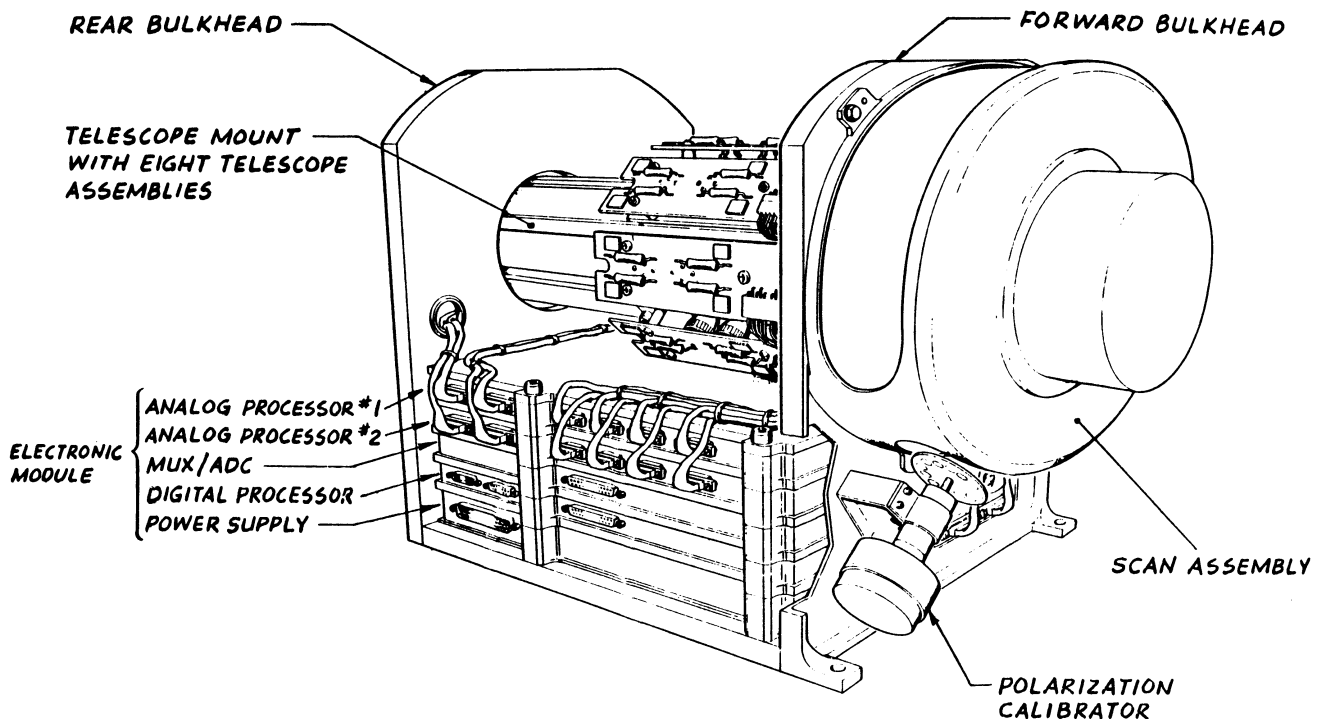


Fig. 1. Cut-away view of the EOSP.

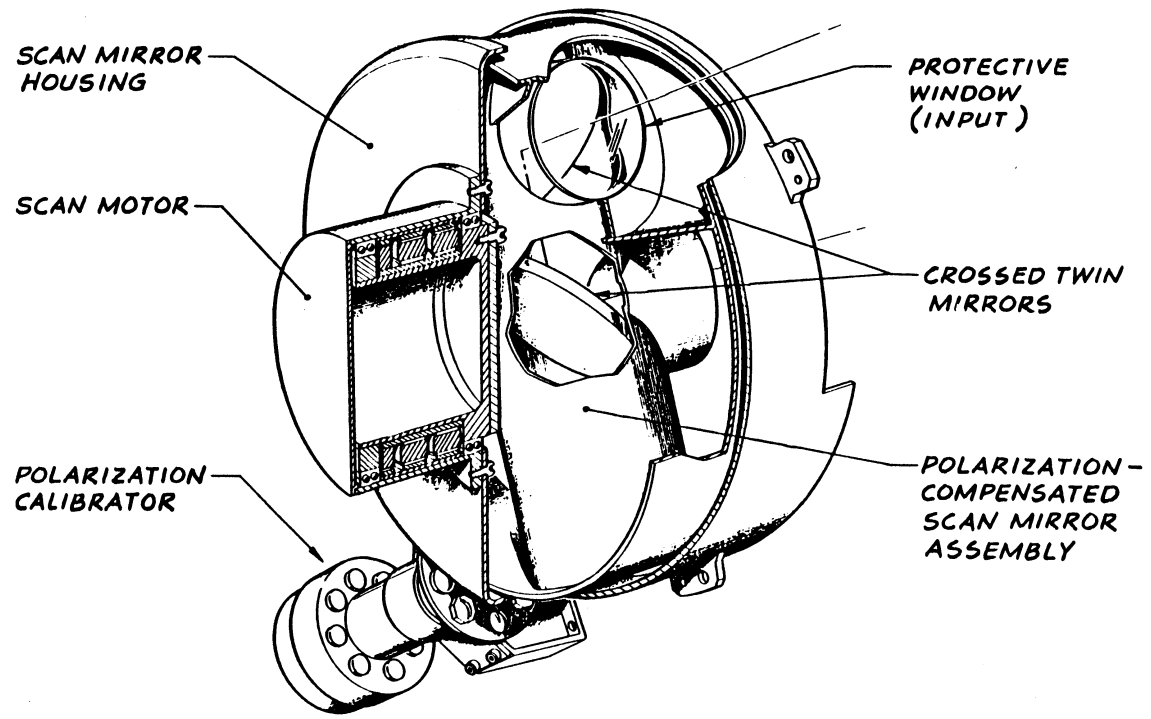


Fig. 2. Schematic representation of twin scan mirror assembly, housing, scan motor, and polarization calibrator.

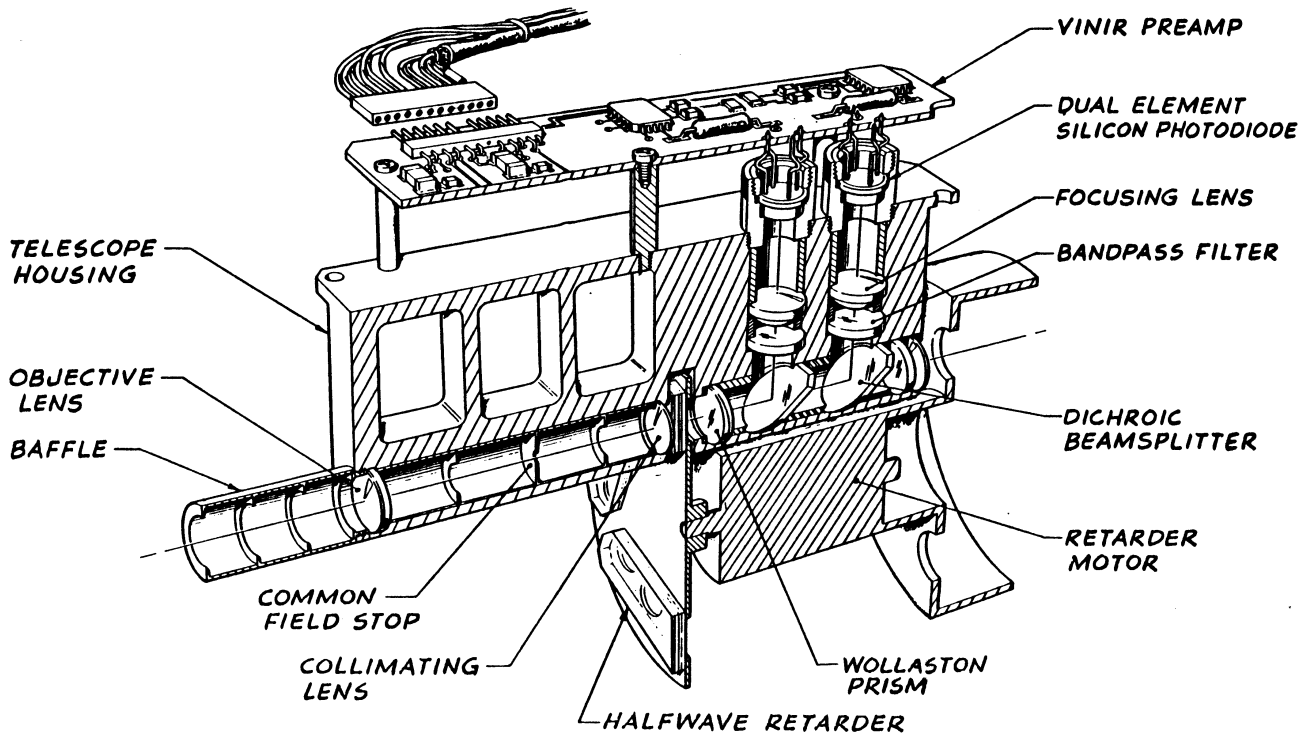


Fig. 3. Schematic of modular EOSP telescope assembly.

However, attention must be paid to potential contamination during flight. Any differential contamination of the two mirrors would mean that they were no longer identical and the cancellation of their respective instrumental polarization components would be degraded, so the carrying tube entrance and exit apertures are covered by fused silica windows to prevent or minimize contaminant access to the mirrors.

Eight boresighted telescope and aft optics assemblies provide the required spatial, spectral and polarization separations of the scanned scene. Each assembly, as illustrated in Fig. 3, contains a baffle system, 1-cm aperture refractive telescope, field stop, relay lens, and Wollaston prism to define the field of view and separate the incident scene flux into two orthogonally-polarized, angularly-separated beams. The beams are then spectrally separated into three spectral bands using two dichroic beamsplitters and three bandpass filters. Telescope foreoptics employ an apochromatic design to maintain the same focal length at the three separate wavelengths for each telescope so that the scene footprint is identical for all of the EOSP spectral bands. Each pair of polarized and spectrally defined beams are focused on either a dual-detector, silicon photodiode detector package (for the eight visible and near infrared [VINIR] spectral bands) or a pair of HgCdTe photodiode detectors located on the cold (185 K) focal plane (for the four shortwave infrared [SWIR] spectral bands).

The telescope and aft optics assemblies are grouped in pairs with the outputs from a detector pair for one telescope providing the 0°/90° polarization azimuths and the outputs from the respective detector pair for the other telescope giving the 45°/135° azimuths. The octagonal telescope mount provides the appropriate configuration to

allow occasional cross-calibration of the detectors measuring orthogonal polarization components by repositioning the retarder wheel on which four achromatic halfwave retarder plates are mounted. When the retarder wheel is rotated by  $45^\circ$  relative to its normal position, the polarization azimuth of the incident scene flux is rotated by twice that angle by the halfwave retarder, thus simply interchanging the roles of a detector pair.

A calibrator assembly attached to the scan mirror assembly housing on the mounting platform side of the mirror assembly axis (cf. Figs. 1 and 2) provides a set of known source polarization and radiance outputs for an end-to-end inflight calibration. As illustrated in Fig. 4, the calibrator employs an eight-position wheel (each position viewed by one of the eight EOSP telescopes) illuminated by flux from eight exit ports of a small integrating cavity with four small tungsten filament lamps, with each lamp separately commandable to provide a range of radiance levels. In the polarization calibration mode, the wheel is stepped so that each telescope views each of the eight positions in turn. Five of these positions employ Rochon polarizers oriented at different azimuths as illustrated, while the three remaining positions include a neutral density filter, a clear fused silica window, and an open aperture. Repeated comparisons of the measurements at the fused silica and open positions will serve as a monitor of any inflight contamination in this portion of the instrument by detecting the effect of potential contaminant deposited on the fused silica window. By performing this calibration cycle periodically, we will be able to use changes in the apparent polarization degree and azimuths relative to the known source values to deduce any polarimetric response changes, i.e., alteration of either the instrumental polarization or linear polarization responsivity.

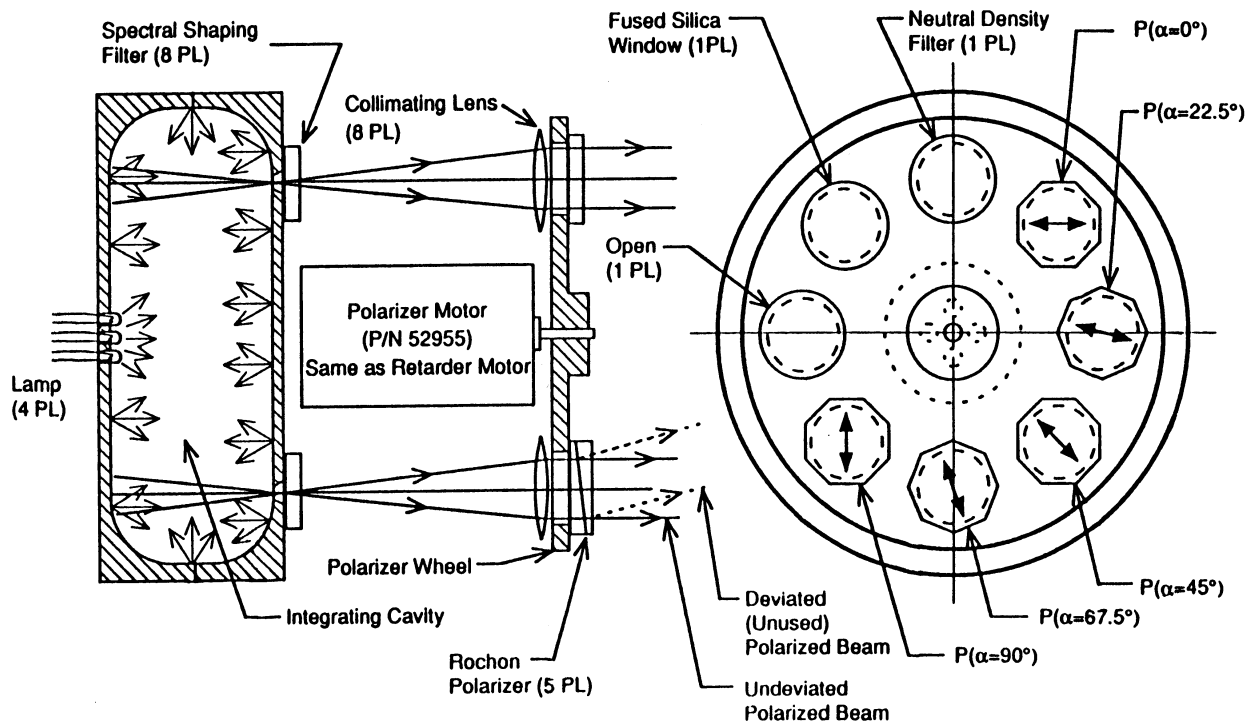


Fig. 4. Schematic of the polarization calibrator assembly.

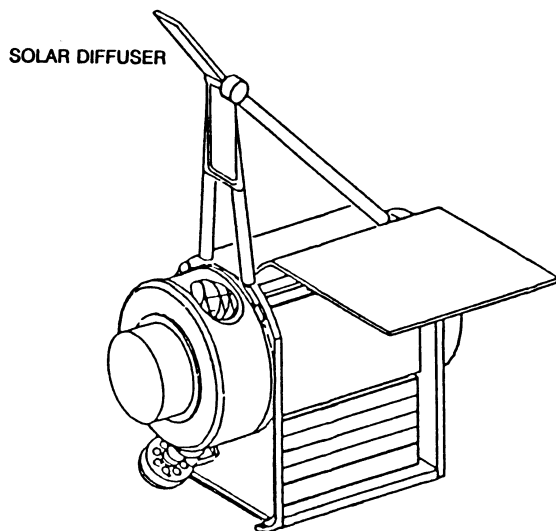


Fig. 5. Schematic representation of solar diffuser assembly attached to the top (nadir side) of the EOSP. Also illustrated is the radiator for the cooled focal plane and the Earth shield in its deployed position.

The required focal plane cooling for the HgCdTe detectors and associated preamplifiers is provided by a single-stage radiative cooler design using a 500 cm<sup>2</sup> radiator on the side of the EOSP facing away from the sun. On a sun-synchronous platform, this "cold" side remains fixed, while for a spacecraft in a precessing orbit, the periodic reorientation of the platform is required. A deployable shield prevents illumination of the radiator by the Earth and in its stowed position during launch, it provides a contamination cover for the radiator. Other than the preamplifiers located with the aft optics, the electronics, which provide command and control, signal processing and formatting, power conditioning, and actuator driver circuitry are located in a module below the octagonal telescope assembly (cf. Fig.1). A solar diffuser assembly, which provides a calibration using a diffuser element illuminated by the sun, is mounted on the top (nadir side) of the EOSP as illustrated in Fig. 5. Upon receipt of the calibration command, the diffuser element is deployed from its normal, stowed position using a

bi-metallic, thermally activated spring mechanism. Two different reflectance standards in strip form (probably Halon with and without carbon filler) are used as diffuser elements to provide two radiance levels.

A key factor in the advantages associated with using polarimetry for remote sensing is the feasibility of producing instruments which can measure the polarization with an accuracy at least an order of magnitude better than is possible for radiance measurements. Accordingly, the EOSP design is based upon the requirement of a minimum signal-to-noise ratio of 2000 at all twelve spectral bands for a typical scene brightness in order to realize this advantage. Table 1 summarizes the basic EOSP instrument characteristics including the predicted signal-to-noise ratio for each band.

### 3. APPROACH

Compared to its use on planetary missions, polarimetric remote sensing has been employed for terrestrial applications in only a very few instances and with limited scope. There have been polarimetric observations from aircraft<sup>13,14</sup> and balloon platforms,<sup>15-18</sup> but the only terrestrial measurements from spacecraft are the photographic polarimetry performed by mission specialists onboard the Space Shuttle.<sup>19</sup> In the absence of multispectral polarimetry observations with substantial spatial and temporal coverage, an approach that relies on actual data to develop scene discrimination and aerosol retrieval techniques cannot be expected to be very successful. Rather, the initial development of retrieval algorithms for potential EOSP observations will employ theoretical simulations of EOSP data using multiple scattering models for varying aerosol-cloud conditions and particle optical properties. The

Table 1. EOSP Instrument Characteristics.

Instrument view:	Cross-track scan, limb to limb			
Instrument IFOV:	14 mrad			
Spectral bands:		$\lambda$ (nm)	$\Delta\lambda$ (nm)	SNR
	VINIR:	410	30	2400
		470	20	3400
		555	20	4200
		615	15	3600
		675	20	4300
		750	15	3300
		880	20	3400
		950	20	3200
	SWIR:	1250	60	4600
		1600	60	3700
		2050	100	3400
		2250	100	2800
Measurement accuracy:	5% absolute radiometric, 0.2% polarimetric			
Data rate:	86 kbps			
Mass:	19 kg			
Size:	54 x 26 x 38 cm			
Power:	15 W (average), 22 W (peak)			

present body of information on cloud and aerosol particle properties and typical variability in vertical distribution based upon *in situ* sampling efforts seems quite adequate to support simulation studies. Even when the routine global remote sensing of aerosols is actually realized, it will almost surely be important to perform frequent validations of retrievals using *in situ* measurements with multiple scattering simulations.

The EOSP instrument is a candidate for flight on the second in the series of EOS AM platforms, which will be in a sun-synchronous orbit with a 10:30 a.m. equator crossing time and at an altitude of 705 km. The scanning mirror assembly of EOSP will sweep the 14-mrad IFOV in the cross-groundtrack direction with a scan rate such that the 10-km IFOV footprints at nadir for successive scans are contiguous. Measurement samples every 14 mrad in scan angle will give approximately 180 scan elements from limb to limb. An important aspect of polarimetric observations is the information content that can be implicit in variations with viewing geometry, particularly the phase angle (sun-object-observer angle). Figure 6 displays contours of phase angle corresponding to the observed points in EOSP scans as a function of scan nadir angle and sub-spacecraft latitude for a solar declination of 0°, i.e., the equinoxes. While there is a latitudinal shift in the contours with season, the essential

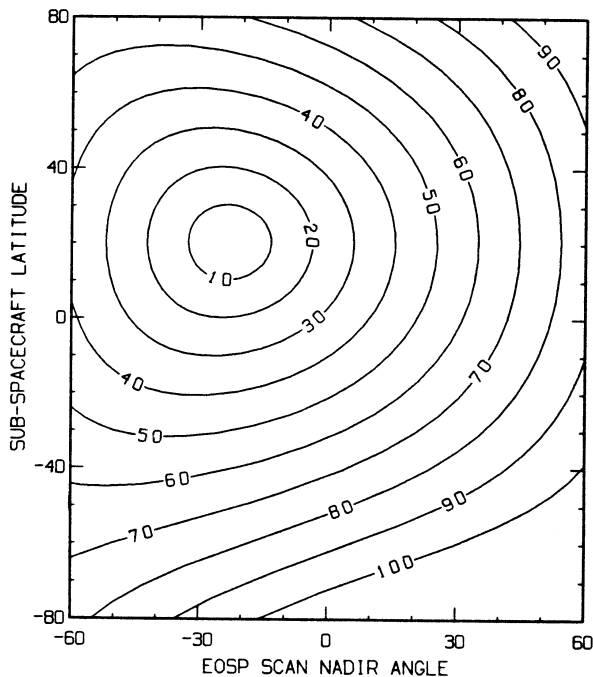


Fig. 6. Contours of phase angle for observed points in EOSP scans as a function of scan nadir angle and sub-spacecraft latitude for EOS polar platform with 10:30 a.m. crossing time.

features remain: middle phase angles ( $\sim 80^\circ$ ) towards the east and smallest phase angles somewhat west of nadir at low latitudes. In performing EOSP data simulations, we calculate the theoretical polarization and radiance for the full range of observing geometries such as represented here for the phase angle coverage.

In most situations, the total opacity of aerosols is small enough so that the surface makes some contribution to the observed radiance and polarization. Over the ocean, the surface reflectivity is low (except for regions close to the sun glint) and relatively predictable, so complications owing to such contributions from the surface are minimized. This is of course the reason that the NOAA operational retrieval of aerosol optical depth is attempted only over ocean. The more challenging situation is over land, where the surface reflectivity and polarization characteristics may be quite variable and not well known *a priori*. Field measurements of the polarization of the scattered sunlight from vegetation suggest that to first order, the polarized component arises almost entirely from the light that is

specularly reflected at the leaf surface.<sup>20</sup> Since the specular reflection can be determined from the Fresnel equations if the refractive index of the leaf is known, an approximation of the expected surface reflectivity and polarization for vegetation may be made using typical spectral properties of plants. Of course, a typical scene over the 10-km IFOV footprint of EOSP will rarely have a uniform plant canopy, but instead can be expected to include different vegetation types as well as contributions due to reflection from soil, sand, and rocks. Although the latter obviously exhibit a spectrally dependent reflectance quite different from that for vegetation, the basic mechanism controlling the polarization signature is likely to be similar for all surface components. Other than for very fine soil or ash with individual particle sizes smaller than the wavelength of observation, the polarized component is probably due primarily to the light specularly reflected, just as for vegetation. The simulation of the polarization and radiance characteristics of the surface for a mixed scene thus requires simply a specification of the mixture and the appropriate refractive indices for the various components.

For a simulation of EOSP data for a vegetation-covered surface, we have used representative leaf refractive indices<sup>21</sup> and computed the polarization assuming that all diffuse scattering is unpolarized. In this particular simulation, the contribution due to non-vegetation components is assumed to be negligible. To simulate the tropospheric aerosol, we adopted aerosol properties corresponding to the continental model of WCP-55,<sup>22</sup> viz., a sulfate component of log-normal distribution with mean radius of

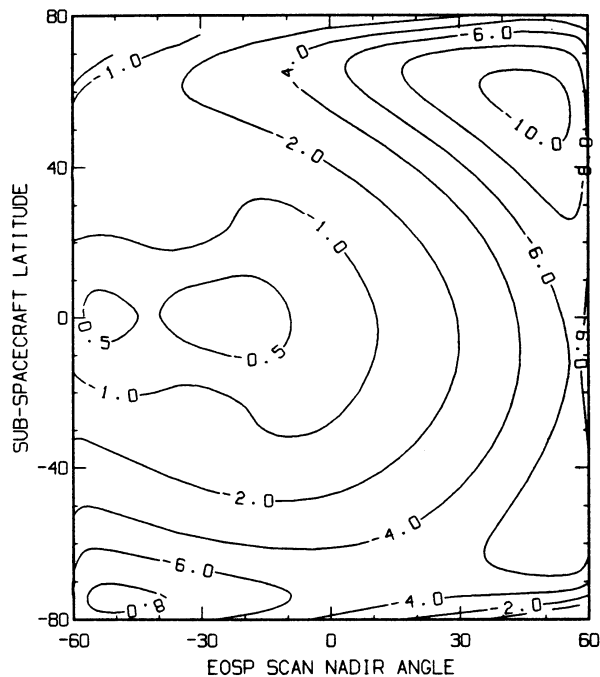


Fig. 7. Contours of the difference in polarization degree for two simulations of EOSP data at 410 nm. The predicted polarization for the model with no aerosol is subtracted from that corresponding to the model with aerosol optical thickness  $\tau=0.15$ .

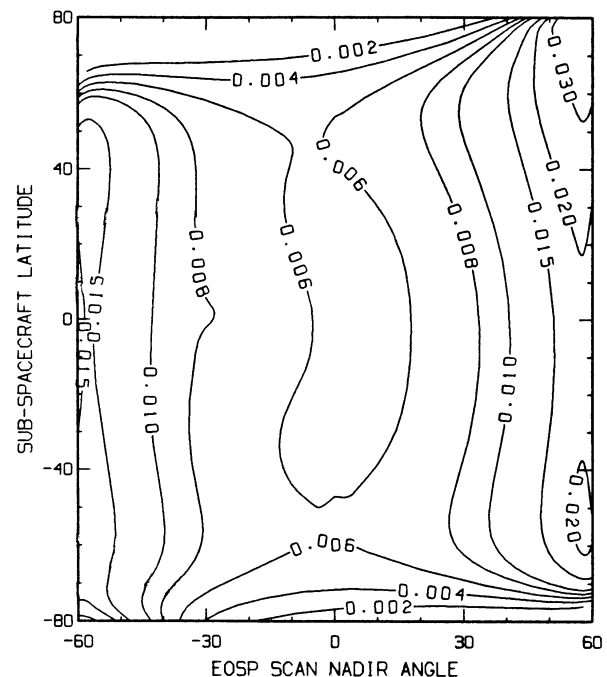


Fig. 8. Contours of the difference in normalized radiance (i.e., reflectance including solar illumination factor) in the same manner as the polarization difference displayed in Fig. 7.

$r=0.15 \mu\text{m}$  and  $\sigma=1.5$ , and a dust component with  $r=0.5 \mu\text{m}$ ,  $\sigma=2.5$ , and a number density 0.003 that of the sulfate component. Simulations at the EOSP spectral bands have been computed for this aerosol with an optical thickness  $\tau=0.15$  at a reference wavelength of 550 nm; the aerosol is confined to a 300-mb layer over the vegetation surface, and the appropriate contribution due to Rayleigh scattering by the atmosphere is included in the multiple scattering computation. A simulation is also generated for no aerosol, i.e., just the Rayleigh scattering contribution above the surface. Figure 7 displays as a function of sub-spacecraft latitude and EOSP scan angle, contours of the resulting polarization degree at 410 nm for the no aerosol case subtracted from that corresponding to the  $\tau=0.15$  aerosol simulation. Note that the difference is everywhere negative, indicating that the aerosol produces a partial depolarization of the strong positive polarization due to Rayleigh scattering (with the surface playing a minor role because of the moderately large Rayleigh optical thickness [0.32] at this wavelength). The same type of difference contours for the normalized radiance (reflectance including the solar illumination factor) are shown in Fig. 8. Not surprisingly, the aerosol produces slightly higher radiances than the clear-sky condition, but the relatively small differences compared to typical instrument radiometric accuracy illustrate the difficulty in retrieving aerosol with just the radiance. In contrast, the differences in polarization degree at most locations except near very small phase angles should be easily detected given the

0.2% polarization accuracy of EOSP. A similar comparison using a simulation with  $\tau=0.3$  indicates that the amount of depolarization is to first order, proportional to the aerosol optical thickness. Thus, for shorter wavelengths where Rayleigh scattering is important, the magnitude of the depolarization provides a reasonably good determination of aerosol optical thickness.

Because of the typical sizes of tropospheric aerosols, the optical thickness over visible and near-infrared wavelengths usually exhibits a decrease with increasing wavelength as the scattering efficiency falls for radius to wavelength ratios becoming much less than unity. There is thus the opportunity to infer some information on aerosol particle size distribution using retrieved optical thickness at several wavelengths. For vegetation, the surface reflectivity becomes fairly high at wavelengths longer than about 700 nm. Also at about this same wavelength range, the contribution due to Rayleigh scattering becomes negligible because of its  $\lambda^{-4}$  scattering efficiency dependence. As a consequence, there is a transition from the situation at shorter wavelengths where aerosol and Rayleigh scattering are dominant, to middle wavelengths where contributions from aerosol and the surface may be of comparable importance, and finally, to the longer wavelengths where the observed radiance and polarization is essentially that for the surface unless the aerosol optical thickness is extraordinarily high. The broad spectral coverage of EOSP is therefore key to the appropriate separation of the three components and thus provides the potential for retrieval of aerosol properties over a wide range of conditions.

#### 4. ACKNOWLEDGEMENTS

The EOSP instrument design was developed by the Santa Barbara Research Center (SBRC) under an EOS Phase B Study, NASA Goddard Space Flight Center Contract NAS5-30756. Co-Investigators F. Gerald Brown and Edgar E. Russell of SBRC are responsible for the basic instrument concept and key design features. The EOS Project, managed by Goddard Space Flight Center, provided instrument development oversight through EOSP Instrument Managers Andrew Dantzler and Mary DiJoseph and supports ongoing algorithm development by the EOSP science team.

#### 5. REFERENCES

1. R.J. Charlson, S.E. Schwartz, J.M. Hales, R.D. Cess, J.A. Coakley, Jr., J.E. Hansen and D.J. Hofmann, "Climate forcing by anthropogenic aerosols," *Science*, Vol. 255, pp. 423-430, 1992.
2. S. Arunachapur, "Satellite remote sensing of atmospheric optical depth spectrum," *Int. J. Remote Sensing*, Vol. 7, pp. 499-514, 1986.
3. C.R.N. Rao, L.L. Stowe and E.P. McClain, "Remote sensing of aerosols over the oceans using AVHRR data: theory, practice and application," *Int. J. Remote Sensing*, Vol. 10, pp. 743-749, 1989.
4. M.D. King, Y.J. Kaufman, W.P. Menzel and D. Tanre, "Remote sensing of cloud, aerosol, and water vapor properties from the Moderate Resolution Imaging Spectrometer (MODIS)," *IEEE Trans. Geosci. Remote Sensing*, Vol. 30, pp. 2-27, 1992.
5. D.J. Diner and J.V. Martonchik, "Atmospheric transmittance from spacecraft using multiple view angle imagery," *Applied Optics*, Vol. 24, pp. 3503-3511, 1985.
6. D. Tanre, P.Y. Deschamps, C. Devaux and M. Herman, "Estimation of Saharan aerosol optical thickness from blurring effects in Thematic Mapper data," *J. Geophys. Res.*, Vol. 93, pp. 15955-15964, 1988.
7. J.E. Hansen and A. Arking, "Clouds of Venus: evidence for their nature," *Science*, Vol. 171, pp. 669-672, 1971.

8. J.E. Hansen and J.W. Hovenier, "Interpretation of the polarization of Venus," *J. Atmos. Sci.*, Vol. 31, pp. 1137-1160, 1974.
9. P.H. Smith and M.G. Tomasko, "Photometry and polarimetry of Jupiter at large phase angles II. polarimetry of the South Tropical Zone, South Equatorial Belt, and the polar regions from Pioneer 10 and 11 missions," *Icarus*, Vol. 58, pp. 35-73, 1984.
10. M.G. Tomasko and L.R. Doose, "Photometry and polarimetry of Saturn from Pioneer 11: observations and constraints on the distribution and properties of cloud and aerosol particles," *Icarus*, Vol. 58, pp. 1-34, 1984.
11. M.G. Tomasko and P.H. Smith, "Photometry and polarimetry of Titan: Pioneer 11 observations and their implications for aerosol properties," *Icarus*, Vol. 51, pp. 65-95, 1982.
12. K. Kawabata, D.L. Coffeen, J.E. Hansen, W.A. Lane, M. Sato and L.D. Travis, "Cloud and haze properties from Pioneer Venus polarimetry," *J. Geophys. Res.*, Vol. 85, pp. 8129-8140, 1980.
13. W.G. Egan, "Aircraft polarimetric and photometric observations," in *Proceedings, Fifth International Symposium on the Remote Sensing of the Environment*, pp. 169-189, Environmental Research Institute of Michigan, Ann Arbor, 1968.
14. D.L. Coffeen and J.E. Hansen, "Airborne infrared polarimetry," in *Proceedings, Eighth International Symposium on the Remote Sensing of the Environment*, pp. 515-522, Environmental Research Institute of Michigan, Ann Arbor, 1972.
15. C.R.N. Rao, T. Takashima and R.B. Toolin, "Measurements and interpretation of the polarization of radiation emerging from the atmosphere at an altitude of 28 km over south-western New Mexico (USA)," *Quart. J. R. Met. Soc.*, Vol. 99, pp. 294-302, 1973.
16. L.L. Stowe, "Polarization of reflected sunlight as measured from a high-altitude balloon," in *Proceedings, Optical Polarimetry, Instrumentation and Applications*, Vol. 112, pp. 176-183, SPIE., San Diego, 1977.
17. M. Herman, J.Y. Balois, L. Gonzalez, P. Lecomte, J. Lenoble, R. Santer and C. Verwaerde, "Stratospheric aerosol observations from a balloon-borne polarimetric experiment," *Applied Optics*, Vol. 25, pp. 3573-3584, 1986.
18. J.L. Deuze, C. Devaux, M. Herman, R. Santer, J.Y. Balois, L. Gonzalez, P. Lecomte and C. Verwaerde, "Photopolarimetric observation of aerosols and clouds from balloon," *Remote Sens. Environ.*, Vol. 29, pp. 93-109, 1989.
19. W.G. Egan, W.R. Johnson and V.S. Whitehead, "Terrestrial polarization imagery obtained from the Space Shuttle: characterization and interpretation," *Applied Optics*, Vol. 30, pp. 435-442, 1991.
20. V.C. Vanderbilt, L. Grant, L.L. Biehl and B.F. Robinson, "Specular, diffuse, and polarized light scattered by two wheat canopies," *Applied Optics*, Vol. 24, pp. 2408-2418, 1985.
21. S. Jacquemoud and F. Baret, "PROSPECT: a model of leaf optical properties spectra," *Remote Sens. Environ.*, Vol. 34, pp. 75-91, 1990.
22. WCP-55, *World Climate Research Program Report of the Experts Meeting on Aerosols and Their Climatic Effects*, WMO, Williamsburg, 1983.

